Energy Proceedings
Vol 54, 2025
ISSN 2004-2965

Field-scale Simulation of Closed-Fracture Acidizing for Acid Etching Patterns and Conductivity Prediction

Panpan Lu [1], Jianye Mou [1,2*], Shicheng Zhang[1,2], Sinan Li [1], Xinliang Wang [1], Xiaoyi Sun [1]
1 Petroleum Engineering Dept., China University of Petroleum, Beijing, 102249, China
2 National Key Laboratory of Petroleum Resources and Engineering Beijing, 102249, China
*Corresponding author: moujianye@cup.edu.cn.

ABSTRACT

Maintaining fracture conductivity in acid-fractured carbonate reservoir presents a significant challenge as the fractures tend to close due to closure pressure. A viable approach to prevent the decline of conductivity is closed-fracture acidizing (CFA). In this study, we introduce a field-scale numerical model to simulate the acid-etching pattern in CFA and its effect on the conductivity of acid-fractured fractures. The accuracy of the CFA model is validated through experiments under identical acid-etched fracture morphology. The simulation results indicate that the morphology of closed fractures determines the acid-etching patterns. When the mean fracture aperture is small ($\leqslant$2 mm), roughness is high (SD>0.05), and the dimensionless correlation length is extensive ($\geqslant$0.05), acid etching becomes non-uniform, forming grooves and channels. In this case, the live acid reaches farther, and the conductivity remains high under closure stress (improved 8 to 33 times compared to before acidizing). Conversely, the acid uniformly etches the fracture surface, the acid treatment distance is short, and the conductivity rapidly decreases, making the acidizing performance negligible. In short, acid tends to flow into areas with the least resistance, and ultimately affecting acid-etching patterns and conductivity.

Keywords: Closed-fracture acidizing; Numerical model; acid-etching pattern; Conductivity prediction

NONMENCLATURE

Abbreviations	
CFA	Closed Fracture Acidizing
Symbols	
b	fracture width
SD	standard deviation of the fracture width
$N(x,y)$	spatially correlated random numbers
μ	viscosity of acid
p	pressure
p_e	reservoir pressure
$\overline{C}$	average acid concentration
k	reservoir permeability
k_g	acid mass transfer coefficient
β	acid dissolution capacity
ρ	rock density
η	proportion of the leak-off acid
σ	closure stress
E	Young's modulus of the rock
ε	rock strain
σ'	effective closure stress
α	fracture surface contact ratio
C_f	fracture conductivity
q	injection rate of acid
x_f	fracture length
h_f	fracture height

1. INTRODUCTION

Currently, with 70% of the world's oil and gas come from carbonate reservoirs, unconventional treatment measures are increasingly being employed to enhance the recovery in these reservoirs. Acid fracturing is commonly used to enhance the penetration distance and conductivity of carbonate reservoirs [1-3]. However, the conductivity of acid-fractured fractures declines rapidly and is difficult to maintain under high closure stress. In practice, CFA is often utilized for some formations to improve the acidizing performance [4, 5]. The CFA technical [6-8] involves injecting acid into closed fractures at matrix acidizing rates. This process creates non-uniform etching, resulting in grooves or channels that deepen and extend the etched areas, the less-dissolved regions act as supports, keeping the grooves or channels open under high closure stress, thereby reducing fluid flow resistance and generating sustainable conductivity. However, the CFA has not yet been studied as an

This is a paper for the 16th International Conference on Applied Energy (ICAE2024), Sep. 1-5, 2024, Niigata, Japan.

independent method to assess its impact on conductivity. This paper aims to investigate the effect of CFA on closed acid-fractured fractures.

The research of conductivity heavily depends on physical experiments and empirical models [9-11]. Experiments primarily focuses on factors, such as rock mechanical characteristics [12, 13], acid properties [14-18], fracture morphology [19-22], and engineering factors [23]. However, both experimental measurements and empirical models have limitations, including their lack of universality and repeatability. However, simulating fracture morphology in research is overly complex, as it demands hard to obtain fracture morphology parameters, becoming a challenge in guiding practices in the oilfield sites. Therefore, there is a pressing need to develop methods specifically simulation for acid-etching patterns and conductivity prediction in different fracture morphology.

This paper aims to develop a field-scale CFA model with sufficiently small grid sizes and sufficiently large overall dimensions to accurately capture the effects of acid-etching pattern after acid-fracturing. This endeavor seeks to minimize discrepancies between experimental-scale and macro-scale. The paper will establish methodologies and assumptions for CFA, investigating acid-fractured morphology how to effect etching pattern. Ultimately, the model will predict fracture conductivity under distinct etching-patterns and enhance the practicality and adaptability of CFA models in field scales.

2. METHODOLOGY

2.1 Physical model

It uses two rough fracture walls to form a physical model. To simplify, the model only considers the main fracture. The control body is set within the fracture, with a length of L, a height of H, and a fracture width of b, which vary over time and space. The x direction is length, the y direction is height and the z direction is width.

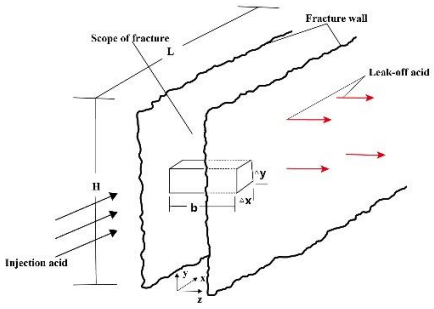

Fig. 1 Physical model

1.1 Model assumptions

(1) The acid is incompressible.

(2) The acid-rock reaction rate is controlled by mass transfer.

(3) Only the effect of the matrix on the leakoff of acid is considered.

(4) Wormholes are ignored.

2.2 The CFA model

Including the continuity, the acid mass transfer, and the fracture width variation equation. These are as follows:

$$\frac{1}{12\mu}\frac{\partial}{\partial x}(b^3\frac{\partial p}{\partial x})+\frac{1}{12\mu}\frac{\partial}{\partial y}(b^3\frac{\partial p}{\partial y})-2\frac{k}{\mu}\frac{p-p_e}{w_m}=\frac{\partial b}{\partial t} \quad (1)$$

$$\frac{1}{12\mu}\frac{\partial}{\partial x}(\overline{C}b^3\frac{\partial p}{\partial x})+\frac{1}{12\mu}\frac{\partial}{\partial y}(\overline{C}b^3\frac{\partial p}{\partial y})-2\overline{C}\frac{k}{\mu}\frac{p-p_e}{w_m} \quad (2)$$
$$-2\overline{C}k_g=\frac{\partial(\overline{C}b)}{\partial t}$$

$$\frac{\beta}{\rho(1-\phi(x,y))}(2\eta\frac{k}{\mu}\frac{p-p_e}{w_m}\overline{C}+2k_g\overline{C})=\frac{\partial b}{\partial t} \quad (3)$$

2.3 Calculation of closed-fracture conductivity

According to the theory of elastic contact, the contact ratio of closed fracture surfaces is calculated by assessing the width of points after deformation occurs at the contact point. If the width of the rock at a point after deformation is less than the minimum fracture width, it is considered that the fracture walls are in contact, thereby calculating the contact ratio of the fracture surfaces. Through iterative calculations, it has been found that increasing closure stress results in a contact ratio of around 0.3 for the fracture surfaces.

$$\sigma=E\varepsilon \quad (4)$$

$$\sigma'=\frac{\sigma}{\alpha} \quad (5)$$

$$\varepsilon=\frac{\Delta b}{b_{\max}-b_{\min}} \quad (6)$$

$$b=b_i-\Delta b \quad (7)$$

According to the *Deng (2011)* model, the numerical model for calculating conductivity is given by equation (8). The pressure field of the closed fracture is computed using the CFA model, and finally, the conductivity of the closed fracture under complex conditions is calculated.

$$C_f = 1.67\frac{q\mu x_f}{h_f \Delta p} \quad (8)$$

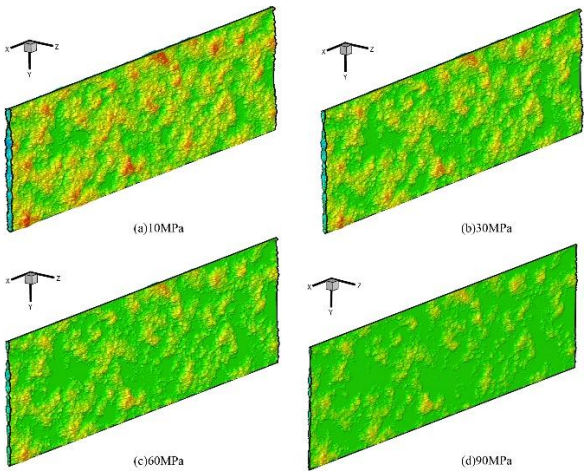

*Fig. 2 Fracture cl*osure morphology under different closure stress

2.4 Initial conditions *and boundary conditions*

Initial conditions are as follows: the pressure within fracture is 0, the acid concentration is 0, and the initial fracture width is generated using the geostatistical software GLSIB.

$$\begin{cases} p(x,y) = 0 \quad \forall x,y,t = 0 \\ \overline{C}(x,y) = 0 \quad \forall x,y,t = 0 \\ b(x,y) = b_{ini}(x,y) \quad \forall x,y,t = 0 \end{cases} \quad (9)$$

Boundary conditions are as follows: at the entrance of the fracture, the injection rate of acid is constant, determining the pressure at this point. The pressure at the outlet of the fracture is equal to the reservoir pressure. Along the upper and lower boundaries of the fracture, the pressure gradient is 0. The acid concentration at the entrance remains at its initial concentration.

$$\begin{cases} \int_0^h \frac{b^3}{12\mu}\frac{\partial p}{\partial x}\Big|_{x=0} dy = q \quad t > 0 \\ p(l,y) = p_e \quad \forall y, t > 0 \\ \frac{\partial p}{\partial y}\Big|_{y=0} = 0 \quad \forall x, t > 0 \\ \frac{\partial p}{\partial y}\Big|_{y=h} = 0 \quad \forall x, t > 0 \\ \overline{C}(0,y) = C_i \quad \forall y, t > 0 \end{cases} \quad (10)$$

The above boundary conditions and initial conditions form the CFA model and conductivity calculation model.

2.5 Numerical solving and model validation

The fracture is discretized into a 400 × 400 grids, and the equations in the model are solved using the finite volume method. A simulation program developed in C++. Due to the short time steps involved, the equations are solved sequentially through coupling. Iterative calculations are repeatedly performed until the injection time is reached, at which the calculations terminate.

The model was validated for correctness and accuracy at the experimental scale. By importing the fracture width distribution from 3D-scanned data into the established model, the changes in conductivity under different closure stresses were calculated. The simulation results showed that the conductivity predicted by this model was consistent with laboratory measured conductivity. Therefore, it can be concluded that the established model accurately reflects the actual acid-etching behavior.

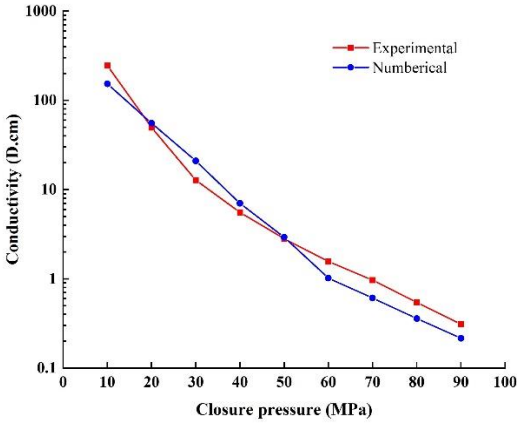

Fig. 3 Comparison of experimental and numerical results

3. RESULT AND DISCUSSION

Table 1 The parament of fracture and acid

Parameter	Value	Parameter	Value
Fracture size	30m× 100m	Acid viscosity (mPa·s)	30
Rock density (kg·m^{-3})	2710	Acid density (kg·m^{-3})	1070
Formation pressure (MPa)	45	Acid dissolution capacity	0.082m^3 (rock)/m^3(acid)
Average reservoir permeability (md)	5	Acid mass transfer coefficient (m·s^{-1})	4×10^{-5}
Porosity	0.2	Acid concentration	20wt%

The initial fracture morphology parameters influence the closed-fracture acidizing performance, ultimately affecting the conductivity of acid-etched

fractures. The fracture and acid parameters used in the closed-acidizing simulation are shown in Table 1.

3.1 Average fracture width

Fluid flow within a closed fracture is influenced by aperture and normal stress, when injecting acid into a closed fracture, the acid tends to migrate towards wider and less resistant regions. When the average fracture width was 0.2mm, a narrow channel formed due to acid etching, allowing the fracture to maintain a higher level of conductivity (1000D.cm) under high closure stress. As the average fracture width increased to 2mm, wide and short grooves were generated, and the effective distance of live acid can reach 70m. After acidizing, conductivity decreased linearly on a semi-logarithmic scale. At 30 MPa, the conductivity improved 15 times compared to before acidizing, increasing to 33.5 times at 60MPa, and further to 80.2 times at 90MPa. Ultimately, the formation of grooves enabled the fracture to maintain a relatively high conductivity(159.7D.cm).

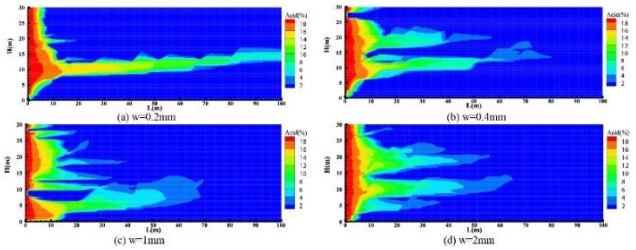

Fig. 4 Acid etching pattern under different average fracture widths

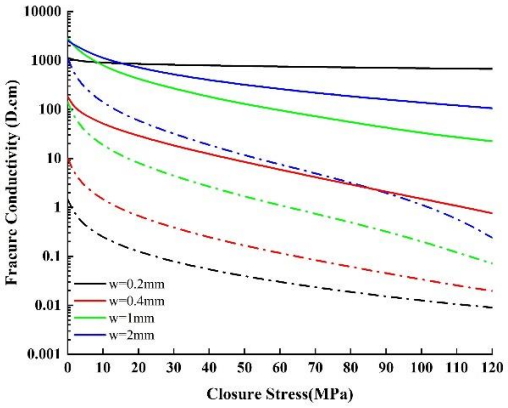

Fig. 5 Variation of conductivity before (dashed line) and after (solid line) CFA

3.2 Fracture surface roughness

The conductivity of CFA results from the combined effects of surface roughness and grooves. On the one hand, the asperities support the fracture surface; on the other hand, the voids between asperities facilitate acid flow, deepening the valleys of asperities to form interconnected etching grooves.

Before acidizing, different roughness possessed a certain level of conductivity. When SD ≤ 0.05 was less than 0.1 D.cm under greater than 35 MPa. When SD is between 0.05 and 0.25, conductivity is less than 100 D.cm under more than 35 MPa; When SD ≥ 0.25, rough fracture surfaces create connected grooves, allowing conductivity to remain high even under significant closure stress. Following to CFA treatment, the conductivity of the fracture depends significantly on the etching patterns. When SD is 0.05, the surface appears relatively smooth, with a uniform acid etching pattern. Under closure stress exceeding 30 MPa, the conductivity measures approximately 0.01 D.cm. With the SD values ranging between 0.05 and 0.25, conductivity improved notably after acidizing; The SD values greater than 0.25, conductivity remains consistently high even under high closure stress. For example, conductivity increased from 36.8 D.cm to 260.2 D.cm(improved 6.1 times) at 30MPa; the conductivity rose from 12.5 D.cm to 116.8 D.cm at 60 MPa(improved 8.3 times); conductivity escalated from 5.3 D.cm to 62.8 D.cm at 90 MPa(improved 10.7 times).

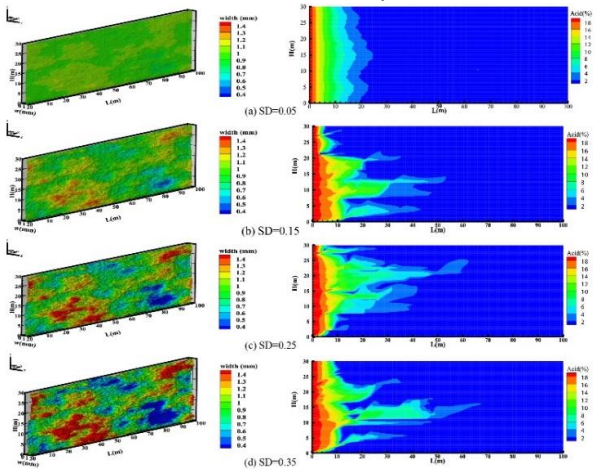

Fig. 6 Initial fracture morphology and distribution of acid concentration under different SD

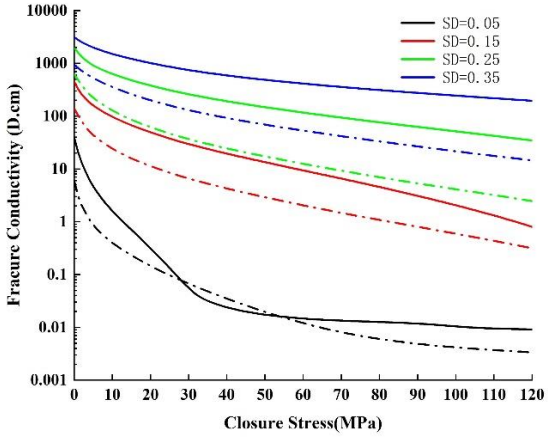

Fig. 7 Variation of conductivity before (dashed line) and after (solid line) CFA under different SD

3.3 Dimensionless correlated length

The dimensionless correlation length influences the orderliness of fracture width distribution within a certain length. If the dimensionless correlation length in a certain direction is smaller, the resulting width is more random, leading to more uniform fracture widths in that direction. Conversely, the heterogeneity increases. In Fig 8 (a), the fracture width distribution is uniform, resulting in a relatively uniform acid-etching pattern. The conductivity decreases to 0.1 D.cm under 60 MPa, because the uniformly dissolved fracture surface closes under high closure stress. As the heterogeneity of the fracture surface increases, the acid etching pattern changes, allowing the conductivity to remain at a relatively high value.

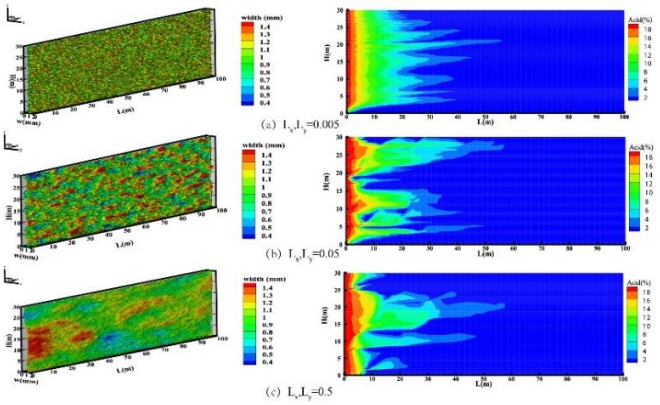

Fig. 8 Fracture surfaces and acid etching patterns with different dimensionless correlation length

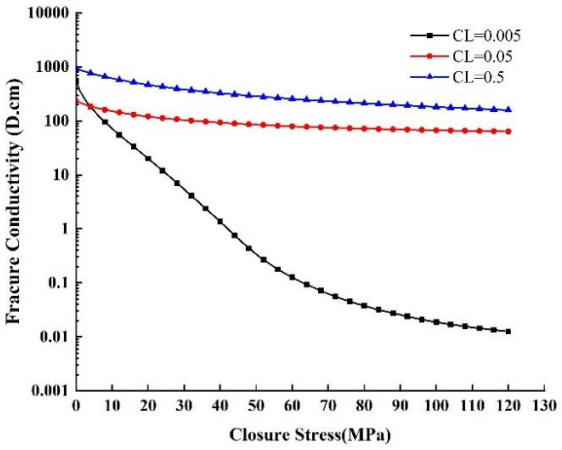

Fig. 9 Variation of conductivity before and after CFA under different correlated length

4. CONCLUSION

By generating acid-fractured fractures using geostatistical methods and coupling the CFA model and conductivity calculation model, we studied the impact of acid-etching patterns on conductivity. The sensitivity analysis of factors influencing conductivity lead to the following conclusions:

(1) The flow path of acid in closed fractures is determined by the fracture width distribution. Smaller average fracture widths facilitate the formation of deeper grooves or channels through acid etching, whereas larger average widths reduce flow resistance, leading to uniform etching on the fracture surface.

(2) Roughness affects the contact ratio of fracture surfaces under closure stress. Smoother surfaces with lower roughness enable uniform acid-etching pattern. As roughness increases, acid etches the surface non-uniformly. When the coefficient of variation increases to 0.35, the voids on the fracture surface can interconnect.

(3) The dimensionless correlation length influences the orderliness of fracture width distribution. Increasing the value in a certain direction enhances the correlation in that direction, resulting in a more homogeneous fracture width distribution.

(4) The grooves or channels generated by non-uniform etching maintain the conductivity of closed fractures at a high level under high closure stress.

REFERENCE

[1] Petriz Munguia J.M., Gonzalez Valtierra B.E., Trujillo Hernandez J., et al. Acid-Fracturing Techniques as a Good Alternative to Help Improve Field Development Assets; proceedings of the Abu Dhabi International Petroleum Exhibition & Conference, F, 2019 [C]. D011S002R003.

[2] Desouky M., Aljawad M.S., Amao A., et al. Chemical Treatment for Sustainable Acid Fracture Conductivity of Weak Carbonates, F, 2023 [C].

[3] Naik S., Dean M., McDuff D., et al. Acid Fracture Conductivity Testing on the Tight Carbonate Ratawi Limestone in the Partitioned Zone, F, 2020 [C].

[4] Sizer J.P., Moullem A.S., Abou-Sayed I.S. Evaluation of Closed Fracture Acidizing Performed in a Tight Limestone Formation; proceedings of the Middle East Oil Show, F, 1991 [C]. SPE-21440-MS.

[5] Pournik M., Mahmoud M., Nasr-El-Din H.A.A. A Novel Application of Closed-Fracture Acidizing [J]. SPE Production & Operations, 2011, 26(01): 18-29.

[6] Fredrickson S.E. Stimulating Carbonate Formations Using a Closed Fracture Acidizing Technique; proceedings of the SPE East Texas Regional Meeting, F, 1986 [C]. SPE-14654-MS.

[7] Sarma D.K., Pal T., Kumar D., et al. Application of Closed Fracture Acidizing for Stmulation of Tight

Carbonate Reservoir in Mumbai Offshore; proceedings of the SPE Oil and Gas India Conference and Exhibition, F, 2017 [C]. D021S007R004.

[8] Aldhayee K., Ali M.T., Nasr-El-Din H.A. Modeling Wormhole Propagation During Closed-Fracture-Acidizing Stimulation in Tight-Carbonate Formations [J]. SPE Journal, 2020, 25(5).

[9] Mou J., Zhu D., Hill A.D.D. New Correlations of Acid-Fracture Conductivity at Low Closure Stress Based on the Spatial Distributions of Formation Properties [J]. SPE Production & Operations, 2011, 26(02): 195-202.

[10] Deng J., Mou J., Hill A.D.D., et al. A New Correlation of Acid-Fracture Conductivity Subject to Closure Stress [J]. SPE Production & Operations, 2012, 27(02): 158-169.

[11] Deng J., Hill A.D., Zhu D. A Theoretical Study of Acid-Fracture Conductivity Under Closure Stress [J]. SPE Production & Operations, 2009, 26(01): 9-17.

[12] Kamali A., Pournik M. Fracture closure and conductivity decline modeling – Application in unpropped and acid etched fractures [J]. Journal of Unconventional Oil and Gas Resources, 2016, 14: 44-55.

[13] Akbari M., Javad Ameri M., Kharazmi S., et al. New correlations to predict fracture conductivity based on the rock strength [J]. Journal of Petroleum Science and Engineering, 2017, 152: 416-426.

[14] He J. An Innovative Closed Fracture Acidizing Technique for Deep Carbonate Reservoirs Using Glda [D], 2015.

[15] Zhang R., Hou B., Zhou B., et al. Effect of acid fracturing on carbonate formation in southwest China based on experimental investigations [J]. Journal of Natural Gas Science and Engineering, 2020, 73: 103057.

[16] He H., Ma X., Lei F., et al. An Experimental Investigation of Interaction between CO_2 Solution and Rock under Reservoir Conditions in the Jimsar Shale Oil Formation [J]. PROCESSES, 2024, 12(4)

[17] Zhu N., Huang W., Gao D. Study on Conductivity of the Etching Fracture via Surface Cross-Linked Acid; proceedings of the 55th US Rock Mechanics/Geomechanics Symposium, F, 2021 [C]. ARMA-2021-1105.

[18] Gou B., Guan C.C., Li X., et al. Acid-etching fracture morphology and conductivity for alternate stages of self-generating acid and gelled acid during acid-fracturing [J]. Journal of Petroleum Science and Engineering, 2021, 200.

[19] Lai J., Guo J., Chen C., et al. The Effects of Initial Roughness and Mechanical Property of Fracture Surface on Acid Fracture Conductivity in Tight Dolomite Reservoir, F, 2019 [C].

[20] Zhang W., Jin X., Zhu D. A Model for Acid Fracture Conductivity Based on Asperity Deformation with Coupled Normal-Shear Behavior of Rough Surfaces, F, 2018 [C].

[21] Asadollahpour E., Baghbanan A., Hashemolhosseini H., et al. The etching and hydraulic conductivity of acidized rough fractures [J]. Journal of Petroleum Science and Engineering, 2018, 166: 704-717.

[22] Lu C., Bai X., Luo Y., et al. New study of etching patterns of acid-fracture surfaces and relevant conductivity [J]. Journal of Petroleum Science and Engineering, 2017, 159: 135-147.

[23] Chen C., Wang S., Lu C., et al. The Impact of Surface Roughness and Injection Rate on Acid-Fracture Conductivity, F, 2021 [C].